remote sensing

MDPI

Article

A Lookup Table-Based Method for Estimating Sea Surface Hemispherical Broadband Emissivity Values (8–13.5 μm)

Jie Cheng [1,*], Xiaolong Cheng [1], Shunlin Liang [1,2], Raquel Niclòs [3], Aixiu Nie [4] and Qiang Liu [4]

1 State Key Laboratory of Remote Sensing, School of Geography, Beijing Normal University, Beijing 100875, China; longtl93111@126.com (X.C.); sliang@umd.edu (S.L.)
2 Department of Geographical Science, University of Maryland, College Park, MD 20742, USA
3 Earth Physics and Thermodynamics Department, University of Valencia, 50 Dr. Moliner, Burjassot E-46100, Spain; Raquel.Niclos@uv.es
4 College of Global Change and Earth System Science, Beijing Normal University, Beijing 100875, China; nieaixiu@126.com (A.N.); toliuqiang@bnu.edu.cn (Q.L.)
* Correspondence: Jie_Cheng@bnu.edu.cn; Tel.: +86-10-5880-7455

Academic Editors: Zhaoliang Li, Richard Müller and Prasad S. Thenkabail
Received: 7 December 2016; Accepted: 3 March 2017; Published: 6 March 2017

Abstract: Sea surface hemispherical broadband emissivity (BBE, 8–13.5 μm) is a vital parameter for calculating surface radiation budgets. Such data are currently unavailable. This paper proposes a lookup table-based method for retrieving sea surface hemispherical BBE values. The physically-based sea surface emissivity model of Wu and Smith, together with the optimal refractive index, were used to generate hemispherical BBE values under wind speeds ranging from zero to 50 m/s. A lookup table of hemispherical BBE values as a function of wind speed was established and used to retrieve sea surface hemispherical BBE values under foam-free conditions. The accuracy of the estimates of hemispherical BBE was 0.003, given a wind speed of zero. The foam effect was explicitly considered. After incorporating the foam effect, hemispherical BBE was expressed as a linear function of the hemispherical BBE values of sea water and foam, weighted by the fraction of foam coverage. With this method, we have produced an hourly sea surface hemispherical BBE product with a resolution of 10 km and global coverage that covers the period from 2003 to 2005, using wind speed data from Modern-Era Retrospective analysis for Research and Applications (MERRA)-2.

Keywords: emissivity; broadband emissivity; refractive index; foam; ocean; thermal infrared remote sensing

1. Introduction

Sea surface thermal-infrared emissivity is an important parameter for retrieving sea surface temperatures (SSTs) from satellite radiometric measurements [1,2]. SST is used as both a prognostic and a diagnostic variable in numerical weather prediction and in global climate modeling. Satellite-retrieved SSTs with an absolute accuracy of 0.3 K is highly desired for applications in climate monitoring and operational oceanography [3]. However, current operational SST products cannot meet this requirement. For example, the standard deviation of MODIS Collection 5 SST products is larger than 0.5 K [4], and the root mean square error of MODIS SST products is larger than 0.7 K for off-nadir viewing [5]. To achieve this goal, the emissivity needs to be determined with an accuracy of 0.5% [6,7].

The oceans play a pivotal role in the global circulation system by storing heat absorbed at low latitudes and redistributing it to higher latitudes. Most of the heat subsequently released to the atmosphere is transferred through the sea surface by sensible and latent heat fluxes and thermal

radiation. Human activity is the primary cause of the Earth's energy imbalance (EEI), which is driving global warming [8,9]. EEI is best estimated from changes in ocean heat content (OHC), complemented by radiation measurements from space [8,10]. As noted by Cheng et al., broadband emissivity (BBE, 8–13.5 μm) is the most suitable spectral range for calculating surface longwave net radiation [11]. However, current BBE data sets are calculated using emissivity values derived from satellite observations at certain view angles, due to the difficulties involved in satellite-based retrieval of emissivity. These data sets actually report directional BBE values. The use of directional BBE values certainly affects the accuracy of estimates of surface longwave net radiation. For example, the error introduced by ignoring the emissivity directionality in estimating surface longwave net radiation can be as high as 17.48 and 14.05 W/m^2 for water and bare ice, respectively, if the sensor scan angle is within $\pm 55^\circ$ [12]. High-quality sea surface hemispherical BBE estimates at 8–13.5 μm will benefit the study of the surface radiation budget and global warming.

A number of studies have been devoted to modeling the thermal infrared emissivity of wind-roughened sea surfaces. Masuda et al. published a model for calculating the emissivity values of pure and sea waters [13]. The sea surface was represented as many facets, whose slopes were described by the isotropic Cox-Munk wave slope distribution function [14] with respect to the surface wind. They tabulated the emissivity in the ranges of 3.5–4.1 μm and 8–13 μm for all view angles. The multiple scattering between facets or surface-emitted surface-reflected (SESR) radiation was not considered in their model. A difference of 0.02–0.03 between the model estimates and in situ measurements was reported at larger emission angles (73.5°). Watts et al. investigated the emission and reflection properties of rough sea surfaces and the role of SESR radiation, which enhances the emissivity value at high wind speeds [15]. Wu and Smith improved the Masuda model by incorporating the process of multiple scattering (the reflection of emission from the sea surface) between facets [16]. Both the Watts model and the Wu and Smith model show increased agreement with a limited set of field measurements over the Masuda model. Later, Masuda revised his model to account for SESR radiation [17]. The discrepancy between the computed and measured emissivity at larger emission angles was significantly reduced by incorporating the SESR emission. In the aforementioned models, the isotropic Cox-Munk wave slope distribution function [14] was adopted. Freund et al. developed the model using anisotropic Cox-Munk wave slope statistics [18]. Henderson et al. developed a model for calculating the polarized emissivity of wind-roughened sea surfaces, using a Monte Carlo ray-tracing method [19]. The effects of both shadowing and the reflected component of the surface emission were included in their model. Nalli et al. developed the surface-leaving radiance model to calculate the surface-leaving infrared radiance. This model includes both emissivity and atmospheric reflection in a systematic yet practical manner [20]. Validation of the model against an exhaustive set of Fourier transform spectrometer (FTS) field observations indicated that the model reduced the bias over standard models at emission angles $\geq 45^\circ$ [21]. A few of the models have gained acceptance in the satellite remote sensing community. For example, the Wu and Smith model is currently used within the Global Data Assimilation System of the National Centers for Environmental Prediction, U.S. National Oceanic and Atmospheric Administration [22]. Even though the physical mechanisms included in the model are improving gradually, the discrepancies between model calculated emissivity values and in situ measurements at greater observation angles and high wind speeds are only partially resolved.

To our knowledge, the ability of the aforementioned models to simulate sea surface hemispherical BBE has not been reported, and foam effects are not included in current models. The objective of this study is to develop a lookup table-based method to produce global, hourly sea surface hemispherical BBE data at a resolution of 10 km to facilitate the study of the sea surface radiation budget. The remainder of the paper is organized as follows: the data used, the wind-roughened sea surface emissivity model and the description of the method developed are introduced in Section 2. The optimization of the refractive index, the validation of the simulated BBE values, and the generation of the global hemispherical BBE product are described in Section 3. Section 4 summarizes the paper and its main conclusions.

2. Data and Methods

In conjunction with high-quality, in situ-measured directional emissivity spectra of the sea surface, the Wu and Smith model was used to determine the optimal refractive index of sea water and to produce directional sea surface emissivity spectra at 8–13.5 μm. The foam-free hemispherical BBE values were derived from these spectra through spectral and angular integration. A lookup table of hemispherical BBE versus wind speed was established for improving computation efficiency in producing the global sea surface hemispherical BBE product. The effects of sea foam were explicitly incorporated by area weighting using the fraction of foam coverage.

2.1. Refractive Index

Refractive index is an important parameter that represents the characteristics of the absorptivity, reflectivity and transmissivity of sea water. The refractive index is one of the key inputs for modeling sea surface emissivity. Although many authors have published data on this refractive index [18,21], the consistency is poor between these data. The refractive index of sea water depends on temperature and salinity. To obtain the refractive index of sea water, salinity and temperature corrections must be applied to the values for pure water. Figure 1 shows the different refractive indices obtained by various authors, including the pure water refractive index obtained by Hale and Querry [23], the sea water refractive index of Friedman [24], the pure water refractive index of Pointer and Dechambenoy [25], the pure water refractive index of Wieliczka et al. [26], the refractive index of Hale and Querry with the salinity adjustment of Friedman (labeled as Masuda [13]), and the real part of Hale and Querry combined with the imaginary part of Segelstein (labeled as Wu and Smith [11,27]). As we can see from Figure 1, the variation in the real part is quite large and can be as high as 0.05 among the different sources; moreover, the variation with respect to wavelength is inconsistent. The variation in the imaginary part is relatively small, and the variation was as high as 0.02. These large differences in the refractive indices will inevitably result in inconsistencies in the simulated emissivity. How to select a suitable refractive index is a difficult problem in real applications.

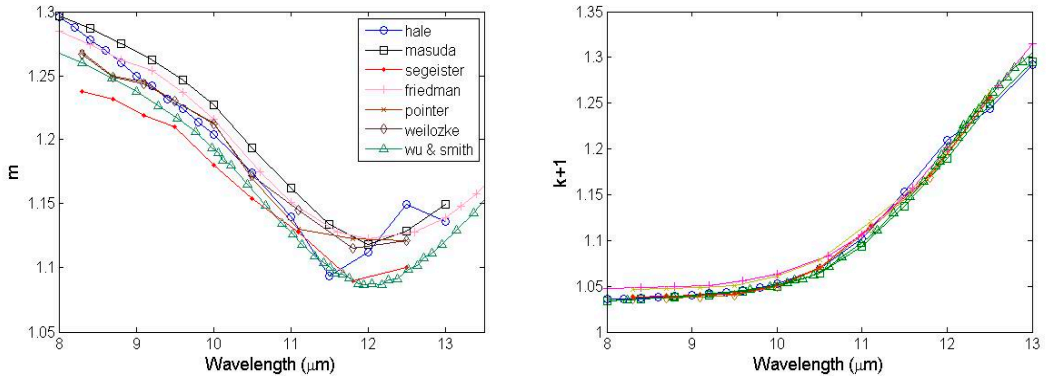

Figure 1. Spectral variation of refractive indices (n = m−ik) obtained from different sources. **Left**: real part; **right**: imaginary part.

2.2. In Situ Measurements

The earliest field-measured sea surface emissivity spectra are those derived from radiometric measurements collected using a high spectral resolution FTS aboard an oceanographic research vessel [28]. On the day of measurement, the sky was clear and the wind speed was approximately 5 m/s for the entire day. The emissivity spectra at three view zenith angles (36.5°, 56.5° and 73.5°) were derived from the FTS measurements. The accuracy of the derived emissivity is believed to be 0.1%. Detailed information on the field measurements and the technique for deriving the sea surface emissivity spectra are provided by Smith et al. [28].

Niclòs et al. measured the sea surface emissivity from a fixed oilrig under open sea conditions in the Mediterranean Sea [29]. The radiometric data were measured using a Cimel Electronique CE 312 radiometer with four channels set to the 8–14 μm range. The sea surface emissivity values were determined for observation angles ranging from 25° to 65° with a step of 5° under wind speeds of approximately 5 m/s and 10 m/s. The accuracy of the derived sea surface emissivity was ±0.004. For detailed information on the field measurements and the technique for deriving the sea surface emissivity, please refer to Niclòs et al. [29,30]. Similar results were obtained using a CE 312 radiometer with six channels placed in the 8-14 μm range [31]. This time a plane sea water sample was measured with the six spectral bands at angles of 15°, 30°, 45°, 50°, 55°, 60°, and 65°. Niclòs et al. also measured the emissivity of foam using a Cimel Electronique CE 312 radiometer [32]. The foam was generated by a network of 104 air diffusers placed at the bottom of a pool filled with sea water and connected to an air pump. The difference between the emissivities measured with foam and under foam-free conditions were about +0.04 for observation angles of 65°.

Branch et al. [33] submerged a porous tube in the bottom of the tank filled with sea water and connected to an air compressor. Foam with an approximate thickness of 2 cm and a maximum bubble diameter of approximately 1 cm was generated. They then conducted an outdoor experiment to measure the emissivity spectra of the generated foam with an FTS for the wavelengths of 3.5–5.5 μm and 8–14 μm and at large observation angles, i.e., incidence angles from 60° to 85°. They also measured the corresponding directional emissivity spectra of foam-free sea water. A complete description of the outdoor measurements and the method for deriving the water and foam emissivity spectra is provided by Branch et al. [33].

As with Wu and Smith [11], the directional emissivity spectra of Smith et al. [28] were used as a reference to determine the most suitable refractive index for sea surface emissivity modeling. The directional BBE of Niclòs et al. [29] and the emissivity spectra of Branch et al. [33] were used to validate the performance of the Wu and Smith model, using the optimal refractive index as an input. The foam emissivities of Niclòs et al. [32] and Branch et al. [33] were combined to correct for the foam effect during the process of generating the global hemispherical BBE product.

2.3. Meteorological Reanalysis Data

Wind speed is an important input to sea surface emissivity models. The wind speed dataset of the second Modern-Era Retrospective analysis for Research and Applications (MERRA-2) is used in the study. The hourly 0.625° × 0.5° eastward and northward wind speeds at 10 m above the sea surface are used to calculate the mean square slope of the facet slope distribution of the wind-roughened sea surface and the hemispherical BBE. The wind speed data used are obtained from the data file abbreviated as M2T1NXSLV in the MERRA-2 data product, which can be downloaded from the following website (ftp://goldsmr4.sci.gsfc.nasa.gov/data/s4pa/).

2.4. Wu and Smith Model

The emissivity of the sea surface is determined by (1) the refractive index of sea water; (2) the sea surface roughness; and (3) the observation angle. A physical model should consider these factors. Figure 2 shows the geometry of emission from a wave facet tangent to the instantaneous sea surface.

The mean emissivity along $\vec{e}$ is the sum of all possible facets and can be described as shown below [13],

$$\bar{\varepsilon}'(\mathrm{n}, \mu_\mathrm{e}) = \frac{1}{\mu_\mathrm{e}} \int_{-\infty}^{\infty} \int_{-\infty}^{\infty} \varepsilon(\mathrm{n}, \chi) cos\chi {\mu_n}^{-1} \times P(z_x, z_y) dz_x dz_y \quad \cos\chi > 0 \tag{1}$$

where $\mu_\mathrm{e} = \cos(\theta_e)$, $\mu_n = \cos(\theta_n)$, $\varepsilon(\mathrm{n}, \chi) = 1 - \rho(\mathrm{n}, \chi)$, $\rho(\mathrm{n}, \chi)$ is the total reflectivity, which can be calculated by Fresnel's formula, and $P(z_x, z_y)$ is the probability density function of the facet slope

distribution of the roughened sea surface. According to Cox and Munk [14], this distribution can be expressed as shown below,

$$P(z_x, z_y) = \frac{1}{2\pi\sigma^2} \exp\left(-\frac{z_x^2 + z_y^2}{2\sigma^2}\right) \tag{2}$$

where σ is the mean square slope. This slope can be calculated from the wind speed w measured at a height of 12.5 m [16], which can in turn be derived from the wind speed at 10 m height [20].

$$2\sigma^2 = 0.003 + 0.00512w \tag{3}$$

Equation (1) can be converted to Equation (4) by replacing the slope increments $dz_x dz_y$ with the angular increments $d\mu_n d\mu_\varphi$,

$$\bar{\varepsilon}'(\mathrm{n}, \mu_\mathrm{e}) = \frac{1}{\pi\sigma^2\mu_\mathrm{e}} \int_0^1 \int_0^\pi \varepsilon(\mathrm{n}, \chi) cos\chi \exp\left(\frac{-\tan^2\theta_n}{2\sigma^2}\right) \times {\mu_n}^{-4} \mathrm{d}\mu_n d\mu_\varphi \quad \cos\chi > 0 \tag{4}$$

Due to wave shadowing, Equation (4) becomes unbounded. Wu and Smith devised a scheme to correct the interwave blocking using a heuristic approach. The mean emissivity is normalized by $\sum(\mu_\mathrm{e})$,

$$\bar{\varepsilon}'(\mathrm{n}, \mu_\mathrm{e}) = \frac{\bar{\varepsilon}'(\mathrm{n}, \mu_\mathrm{e})}{\sum(\mu_\mathrm{e})} \tag{5}$$

where $\sum(\mu_\mathrm{e}) = \frac{1}{\pi\sigma^2\mu_\mathrm{e}} \int_0^1 \int_0^\pi cos\chi \exp\left(\frac{-\tan^2\theta_n}{2\sigma^2}\right) \times {\mu_n}^{-4} \mathrm{d}\mu_n d\mu_\varphi, \quad \cos\chi > 0.$

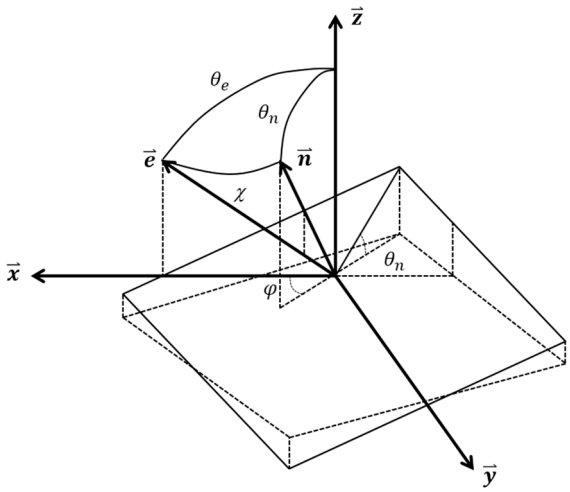

Figure 2. Geometry of emission from a wave facet tangent to the instantaneous sea surface, after Wu and Smith [16]. z is the local zenith; the other two orthogonal components of the Cartesian coordinate system, x and y, are defined such that $\vec{e}$, the unit vector of the emission, is in the x-z plane. $\vec{\mathrm{n}}$ is the facet unit normal vector; θ_n and φ are its zenith and azimuth angles, respectively; θ_e and χ are zenith angles of emission $\vec{e}$ relative to the local zenith z and the facet norm $\vec{\mathrm{n}}$, respectively.

To account for the contribution of the radiance emitted by the sea surface reflecting back on itself, which is significant at high observation angles and wind speed values, the effective emissivity can be defined as

$$\tilde{\varepsilon}(\mathrm{n}, \chi) = \varepsilon(\mathrm{n}, \chi) + [1 - \varepsilon(\mathrm{n}, \chi)] P(\theta_r) \bar{\varepsilon}(\mathrm{n}, \mu_r) \tag{6}$$

where $P(\theta_r)$ is the probability that radiance arriving at this point with a local zenith θ_r originates from the sea surface, rather than from the sky, and $\bar{\varepsilon}(\mathrm{n}, \mu_r)$ is the mean emissivity of the sea surface that

contributes to the radiance emitted at this angle. The effective emissivity $\widetilde{\varepsilon}(\mathrm{n},\chi)$ can then be substituted for $\varepsilon(\mathrm{n},\chi)$ in Equation (4) to produce the final emissivity.

2.5. Description of Our Method

Figure 3 shows the flowchart for estimating sea surface hemispherical BBE in this study. As mentioned in Sections 2.1 and 2.2, publicly available, in situ-measured sea surface emissivity spectra are highly scarce and the refractive indices obtained from various sources are inconsistent. The first issue that must be resolved is to determine which source of refractive index values is most suitable for simulating sea surface emissivity. The in situ directional emissivity spectra measured by Smith et al. [28] are selected as the reference data, based on their high quality and wide acceptance. The Wu and Smith model was then adopted, given its ability to accurately reproduce effective emissivities at any wind speed and at observation angles less than 50° [16,29]. Finally, the most suitable refractive index is determined through optimization, i.e., the refractive index that produces the smallest difference between the simulated emissivities and in situ measurements is the most suitable refractive index.

Given the wind speed from in situ measurements, the observation angle and the optimal refractive index, we can simulate the directional emissivity spectra using the Wu and Smith model. The simulated directional emissivity spectra were converted to a broadband emissivity (8-13.5 μm) by wavelength integration using Equation (7) [11],

$$\varepsilon_{BB}(\mu) = \frac{\int_{\lambda 1}^{\lambda 2} \varepsilon_{\lambda}(\mu) B_{\lambda}(\mathrm{T}_s)\mathrm{d}\lambda}{\int_{\lambda 1}^{\lambda 2} B_{\lambda}(\mathrm{T}_s)\mathrm{d}\lambda} \tag{7}$$

where $\varepsilon_{BB}(\mu)$ is the BBE at observation angle θ; $\lambda 1$ and $\lambda 2$ are the lower and upper bounds of the integration; $B_{\lambda}(\mathrm{T}_s)$ is the Planck's function at surface temperature T_s, which is usually set to 300 K. The BBE uncertainties are less than 0.5% for temperatures ranging from 270 K to 330 K, because BBE is insensitive to common variations in surface temperatures [34]. The hemispherical emissivity is the integration of the upward component of the emitted radiance over the upward hemisphere [35]. Thus, the hemispherical BBE can be derived from $\varepsilon_{BB}(\mu)$ using the formula given below [36],

$$\varepsilon_H = 2\int_0^1 \varepsilon_{BB}(\mu)\mu d\mu \tag{8}$$

where ε_H is the hemispherical BBE that should be used in calculating the surface energy balance. The in situ-measured emissivity data described in Section 2.2 were used to validate the derived hemispherical BBE.

The double integral in the Wu and Smith model means that the process of deriving hemispherical BBE is time consuming, which makes it impossible to carry out global mapping. In fact, the hemispherical BBE is only a function of wind speed if the refractive index, the wave facet slope model and the spectral range of interest are given. If the hemispherical BBE varies monotonically with wind speed, we can establish a lookup table of wind speed and hemispherical BBE and use it to retrieve hemispherical BBE values from wind speeds provided by meteorological reanalysis data under foam-free conditions. Thus, a lookup table provides an alternative method, given its high computational efficiency and acceptable accuracy.

At larger observation angles, the foam emissivity is larger than the sea water emissivity, and reduces the angular variation of sea water emissivity [32]. The foam effect must be considered in the final hemispherical BBE product when the wind speed is larger than 10 m/s [29]. There are many models that can be used to calculate foam coverage from wind speed [37]. Here, we adopted the formula given below to calculate foam coverage [38],

$$F_{foam} = 1.7 \times 10^{-6} {w_{10}}^{3.75} \tag{9}$$

where w_{10} is the wind speed at 10 m, obtained from the MERRA-2 reanalysis data. The hemispherical BBE of foam-covered sea surfaces can be expressed as

$$\varepsilon = F_{foam}\varepsilon_{foam} + (1 - F_{foam})\varepsilon_H \quad (10)$$

where ε_{foam} is the hemispherical BBE for foam that is derived from the measurements reported by Niclòs et al. [29] and Branch et al. [33]. Niclòs et al. measured the directional BBE (8–14 μm) of sea foam for observation angles of 0° and 25°–65° with a step of 5° [29]. Branch et al. measured the directional BBE (8–14 μm) of foam for observation angles of 60°–85° with a step of 5°, as well as 82.5° [33]. Note that the spectral range of BBE is 8–13.5 μm, the spectral range discrepancy between BBE and in situ-measured emissivity will be discussed in later part. The differences are 0.0059 and 0.0185 for observation angles of 60° and 65°, respectively. Niclòs et al. also proposed a quadratic regression function for considering the effect of foam on the emissivity of sea water as a function of the observation angle that is appropriate for angles up to 65° [32]. Compared to the measurements of Branch et al. [26], the quadratic regression function yielded large errors when extrapolated to larger observation angles (>65°). Therefore, we combined the two measurement datasets to produce a complete set of directional BBE values for sea foam by averaging the values from overlapping observation angles, and the results are shown in Figure 4. The hemispherical BBE of foam was calculated using Equation (8), and the corresponding value was 0.9570.

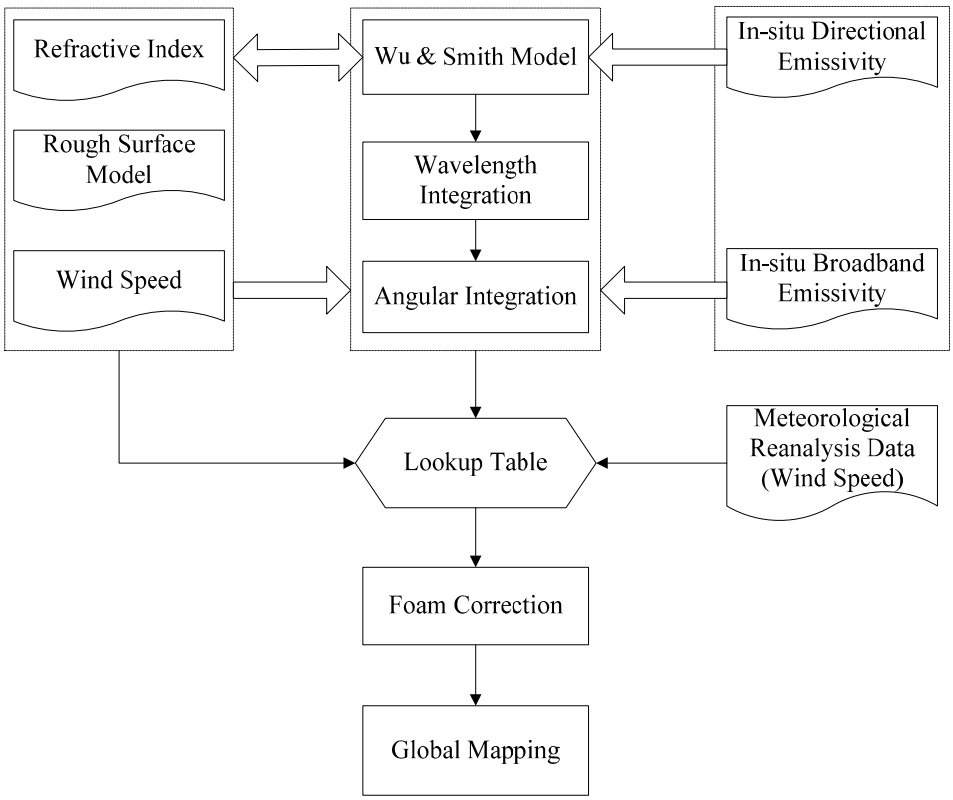

Figure 3. Flowchart describing the procedure for estimating global sea surface hemispherical broadband emissivity.

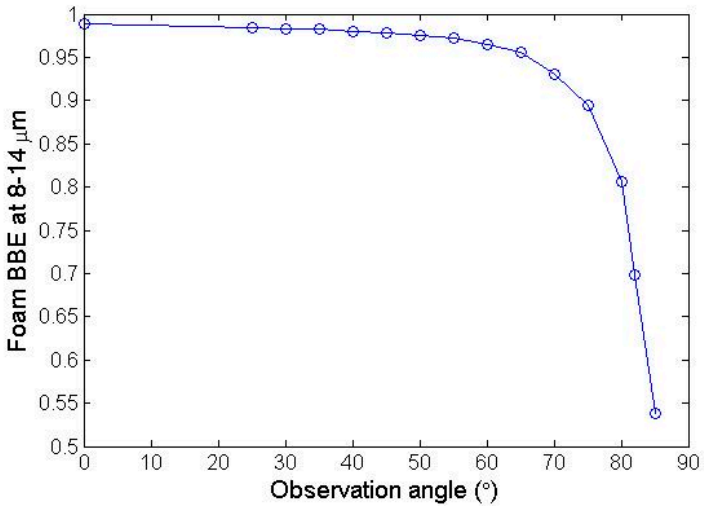

Figure 4. Scatterplot of foam broadband emissivity (BBE) with respect to the observation angle.

3. Analysis of the Results

3.1. Determining Optimal Sea Water Optical Constants

As shown in Figure 1, the real part of the Masuda refractive index was larger than that of Wu and Smith. Meanwhile, the imaginary parts of their refractive indices were close to each other. We simulated the directional emissivity spectra using the Wu and Smith model, based on the above refractive indices. Figure 5 shows the simulation results. The Wu and Smith model achieved better results at view zenith angles of 36.5° and 56.5° using the refractive index of Masuda, but poor results were obtained at a view zenith angle of 73.5. Replacing the refractive index of Masuda with that of Wu and Smith, better results were obtained at a view zenith angle of 73.5, but the simulation results at view zenith angles of 36.5° and 56.5° were not satisfactory. We tried the remaining refractive indices in Figure 1 individually, and did not obtain satisfactory simulation results for the three observation angles at the same time. We also attempted to derive the optimal refractive index using the shuffled evolution (SCE-UA) method [39] and employing the existing refractive indices as initial values, but again, no satisfactory results were obtained. The mechanistic description embedded in the model may be incomplete, or the accuracy of the in situ measurements at different angles may be inconsistent. It is difficult to determine the exact reasons. Finally, we averaged the refractive indices of Masuda and Wu and Smith, and a balanced result was obtained, i.e., the differences between the simulated emissivity spectra and the in situ measurements at each observation angle are acceptable. Table 1 provides the bias and RMSD at each observation angle. The absolute bias and RMSD values are all less than 0.006. The average bias and RMSD for the three observation angles are −0.0009 and 0.003, which is better than the results obtained using the refractive indices shown in Figure 1 individually.

Table 1. The bias and RMSD values of the simulated sea surface emissivity values, using the average of the Wu and Smith and Masuda refractive indices.

Angle (°)	36.5	56.5	73.5
bias	0.0019	0.0012	−0.0058
RMSD	0.0021	0.0014	0.0059

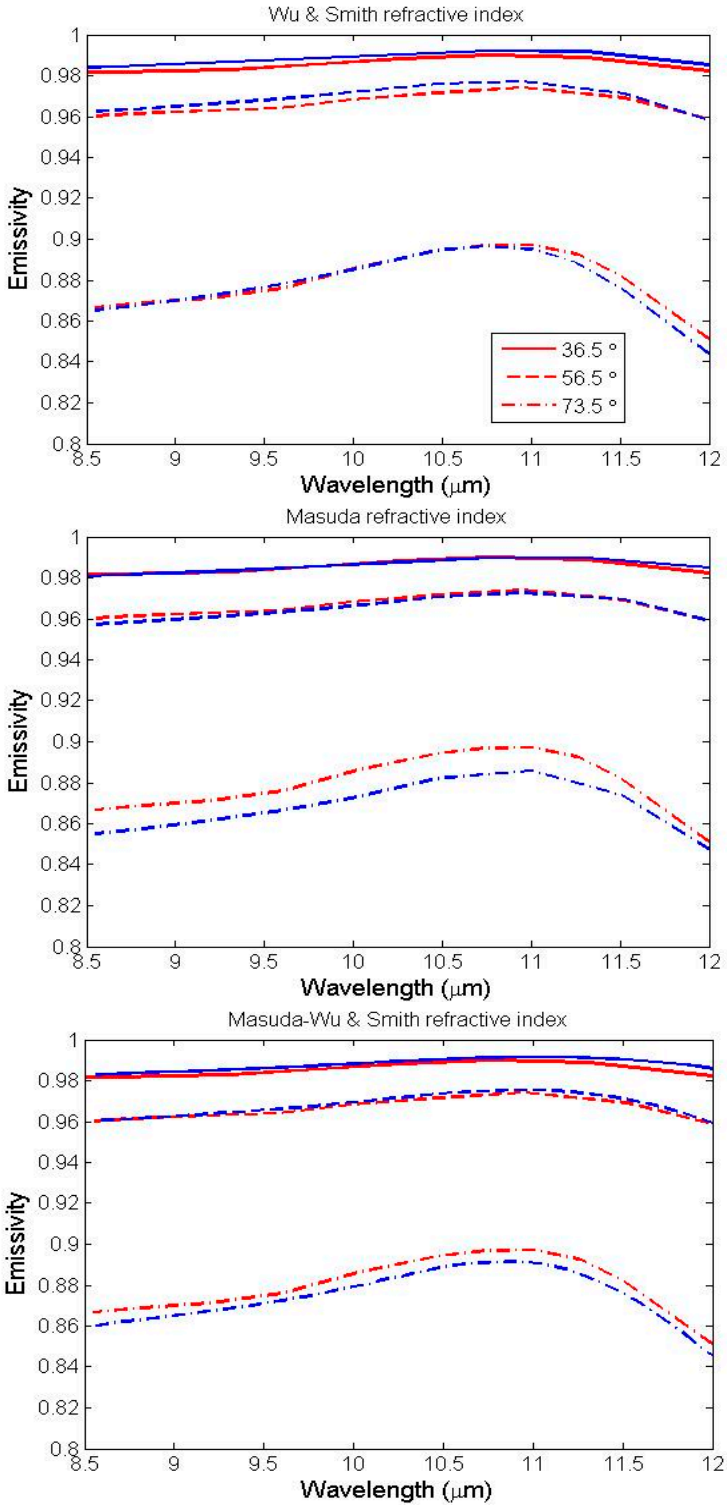

Figure 5. Comparison between in situ-measured sea surface emissivity spectra (red) and those simulated using the Wu and Smith model and the refractive indices from Wu and Smith, Masuda, and the average of Wu and Smith and Masuda (blue). The wind speed is set to 5 m/s.

3.2. Validation of the Simulated Directional and Hemispherical BBE

The in situ sea surface directional BBE (8–14 μm) of Niclòs et al. [29] were used to validate the BBE values simulated using the Wu and Smith model and the optimized refractive index. First, the

emissivity spectra at 8–14 μm were simulated and then converted to a broadband emissivity using Equation (7). The results are compared in Figure 6. The simulated BBE values agreed well with the in situ measurements when observation angles varied from 25° to 65° under wind speeds of 5 m/s and 10 m/s, respectively. The difference between the simulated and measured BBE values ranged from −0.0028 to 0.0019 when the wind speed was 5 m/s, and the difference ranged from −0.0008 to 0.0019 when the wind speed was 10 m/s. The bias and RMSD values were 0.0004 and 0.002 when the wind speed was equal to 5 m/s, and the values were 0.0008 and 0.0014 when the wind speed was 10 m/s. These differences are lower than the uncertainty in the measured BBE values, which is approximately 0.004 [29].

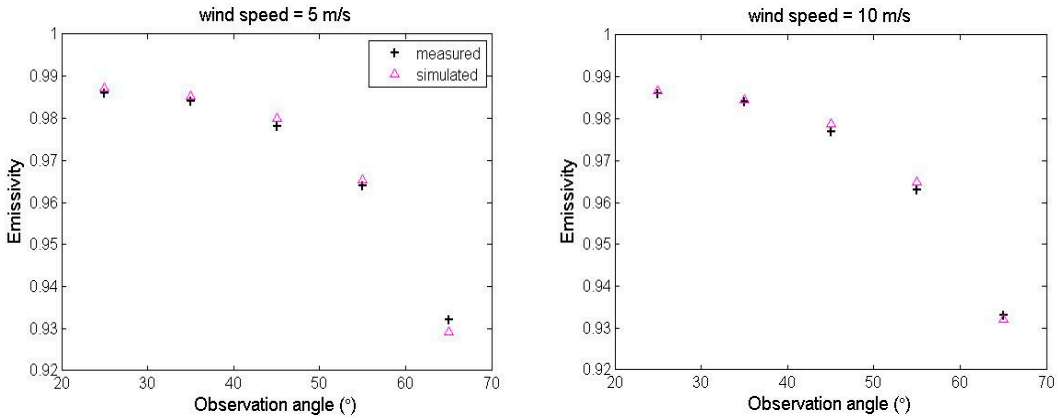

Figure 6. Comparison between the measured and simulated directional BBE values at 8–14 μm.

Figure 7 shows a comparison between the simulated angular emissivity spectra of the sea surface and the in situ emissivity spectra of Branch et al. [33] at large observation angles. They are consistent with each other when the observation angles are equal to 60° and 65°. The absolute difference becomes larger at greater observation angles. The absolute difference is the largest when the observation angle reaches 85°. According to the actual spectral range of the in situ measurements, we calculated the bias and RMSD for each observation angle (Table 2). The simulated emissivity was substantially overestimated at observation angles of 80° and 85°, particularly at an observation angle of 85°. The differences for the remaining angles were very small.

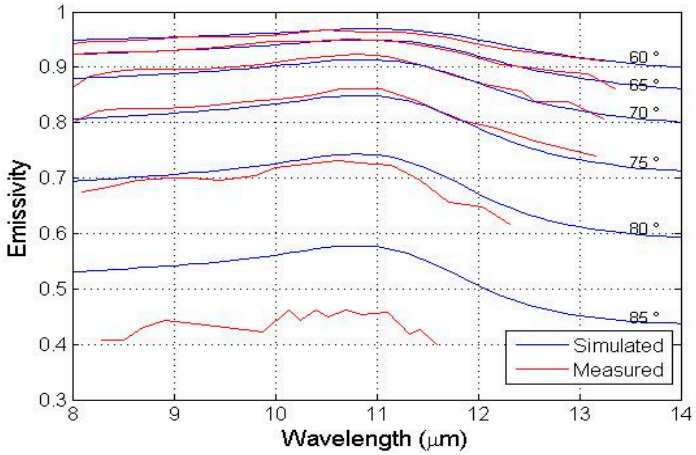

Figure 7. Comparison between simulated emissivity spectra and those measured by Branch et al. [33] at different angles.

Table 2. The bias and RMSD values associated with the simulated sea surface emissivity spectra with respect to in situ measurements.

Angle (°)	60	65	70	75	80	85
bias	0.0038	−0.0007	−0.0044	−0.0094	0.0166	0.1203
RMSD	0.0047	0.0047	0.0086	0.0113	0.0198	0.1247

Combining the results shown in Tables 1 and 2, the absolute bias of the Wu and Smith model in conjunction with the optimal refractive index was less than 0.005 when the observation angle was less than 70°. However, the bias values reflect less accurate results when the viewing angles increase and are larger than 0.005 when viewing angle is larger than 73.5°. This accuracy can meet the requirements of sea surface temperature retrievals; the scan angles of conventional polar orbit satellite sensors like MODIS and AATSR can reach approximately 65°, allowing for the Earth's curvature. Regarding the infrared radiometers on geostationary satellites, which observe sea surface temperatures with large viewing angles (>70°) over the high-latitude ocean, the 0.3 K accuracy of SST retrievals cannot be guaranteed.

We integrated the measured and simulated emissivity spectra into broadband emissivity values at the effective spectral range of measured emissivity spectra. The differences are 0.0039, −0.0014, −0.0058, −0.0094, 0.0158 and 0.128 for observation angles of 60°, 65°, 70°, 75°, 80° and 85°. Assuming that the error of directional BBE values simulated under zero wind speed is less than the results shown in Figure 6, we set the error of directional BBE simulation to be 0.002 when the observation angle is less than 60°. The errors were set to the bias values in Table 2 when the observation angle was larger than 60°. Then, we can calculate the hemispherical BBE approximately from the simulated directional BBE and the hemispherical BBE containing the error assumed above using Equation (8). The corresponding hemispherical BBE values were 0.9472 and 0.9506. The difference is 0.0034.

3.3. Mapping Global Ocean Hemispherical BBE

We simulated the sea surface emissivity at 8–13.5 μm for wind speed values ranging from zero to 50 m/s and then calculated the corresponding hemispherical BBE values using the steps described in Section 2.5. A scatterplot showing hemispherical BBE values versus wind speed is shown in Figure 8. The hemispherical BBE is a univariant function of wind speed and increases monotonically with wind speed. The hemispherical BBE ranges from 0.945 to 0.961. It is difficult to fit this relationship accurately with a simple function. A lookup table of hemispherical BBE versus wind speed was established. The sea surface BBE was interpolated from the lookup table with the input of wind speed at 10 m height derived from MERRA-2 reanalysis data.

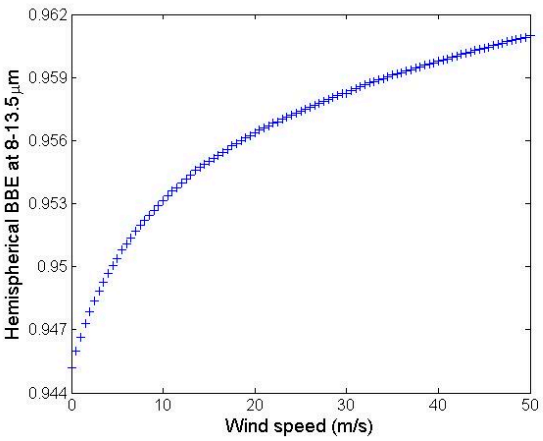

Figure 8. Scatterplot of hemispherical BBE with respect to wind speed.

The hemispherical BBE of each sea surface pixel was calculated using Equation (10). Using 424 representative emissivity spectra that were selected from the ASTER spectral library, the MODIS UCSB spectral library and our soil samples, we calculated the BBE for the 8–13.5 μm and 8–14 μm spectral ranges. The difference is 0.001. Thus, the difference in the BBE of foam between the 8-13.5 μm and 8–14 μm spectral ranges was ignored in this study.

Figure 9 shows a global map of the wind speed data at a spatial resolution of 10 km, which was interpolated from the MERRA-2 reanalysis data at 12:30 (UTC time) on July 1, 2003, using the bilinear method. The produced sea surface hemispherical BBE values are shown in Figure 10. Compared to the hemispherical BBE values produced using the original MERRA-2 wind speed data, the interpolation of the wind speed data does not provide additional information; instead, it facilitates the calculation of the sea surface radiation budget at a higher spatial resolution. As shown in Figures 9 and 10, the spatial pattern of hemispherical BBE values agrees well with that of the wind speed data. High wind speeds correspond to larger hemispherical BBE values, and vice versa.

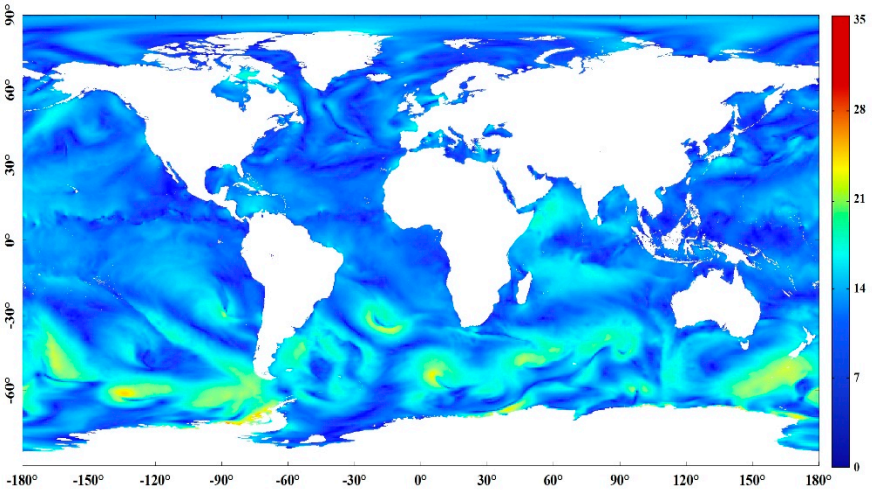

Figure 9. Map of global wind speeds (m/s) at 12:30 (UTC time) on 1 July 2003.

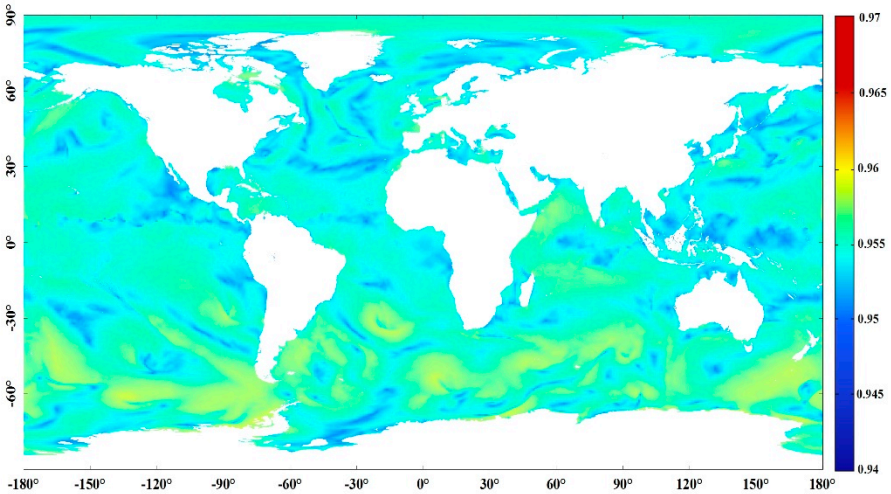

Figure 10. Map of global sea surface hemispherical BBE values at 12:30 (UTC time) on 1 July 2003.

We have produced a data set containing global hourly sea surface hemispherical BBE values with a resolution of 10 km that covers the period from 2003 to 2005 using the interpolated wind speed data. The mean global sea surface hemispherical BBE values at 12:30 (UTC time) for 2003–2005 are shown in Figure 11. Mean hemispherical BBE has a clear dependence on latitude; it is low in the

polar regions and the equatorial regions, and it is high in the mid-latitude regions, especially in the Southern Hemisphere.

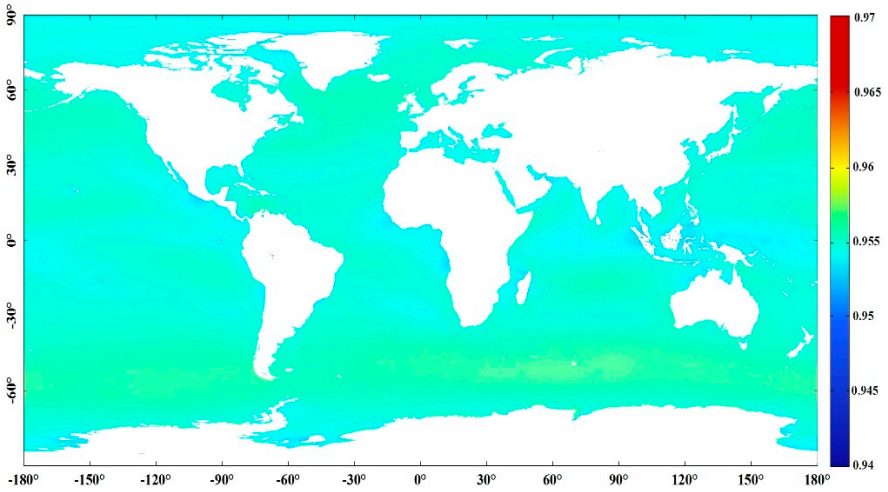

Figure 11. Mean global sea surface hemispherical BBE values at 12:30 (UTC time) from 2003 to 2005.

4. Discussion

Even though scientists have realized that the emissivity of ocean surface varies with the viewing zenith angle and the sea state long before, a constant emissivity value is adopted in calculating surface radiation budget. An emissivity value of 0.986 is assigned to water for the Clouds and the Earth's Radiant Energy System (CERES) window channel (8–12 μm) for calculating surface longwave radiation budget [40]. The BBE over ocean is set to 0.971 in the algorithm developed for retrieving surface upward longwave radiation from the Geostationary Operational Environment Satellite-R Series (GOES-R) Advanced Baseline Imager (ABI) [41]. According to this study, the hemispherical BBE ranges from 0.945 to 0.961. A 0.01 error in BBE introduces 4.59 W/m2 error in the estimate of surface upward longwave radiation assuming surface temperature is 300 K and surface downward longwave radiance remains unchanged. Obviously, a more realistic BBE data set will greatly improve the accuracy of the surface radiation budget. To our knowledge, this is the first time that sea surface hemispherical BBE has been provided. We believe it will benefit the study of the sea surface energy budget and global change.

5. Conclusions

This paper proposes a lookup table-based method for retrieving sea surface hemispherical BBE values. In conjunction with high-quality in situ-measured directional emissivity spectra of the sea surface, the Wu and Smith model was used to determine the optimal refractive index of sea water and to produce directional sea surface emissivity spectra at 8–13.5 μm, from which the foam-free hemispherical BBE was derived through spectral and angular integration. The accuracy of hemispherical BBE simulation is 0.003 under zero wind speed conditions. A lookup table of hemispherical BBE versus wind speed was established for improving the computational efficiency in producing a global sea surface hemispherical BBE product. The effect of sea foam was explicitly incorporated by area weighting using the fraction of foam coverage. With this method, we have produced a global hourly sea surface hemispherical BBE data product with a resolution of 10 km covering the period from 2003 to 2005 using wind speed values interpolated from the MERRA-2 reanalysis data. To our knowledge, this is the first time that sea surface hemispherical BBE has been provided. In addition, the foam effect was explicitly incorporated. We believe this work will benefit the study of the sea surface energy budget and global change.

Three aspects of this study can be improved in the future. (1) The refractive index. Many refractive indices for pure and sea water have been published since the 1960s [42]. Large disparities still exist among these indices, due to the different measurement techniques, experimental configurations, and methods for correcting for temperature and salinity dependence that have been used [6,16,43,44]. More studies should be carried out to determine the most suitable refractive index values for pure and sea water for use in modeling infrared emissivity. (2) The rough sea surface emissivity model. Effort should also be devoted to improving the model's accuracy at large observation angles and high wind speeds. (3) The model validation. The model for estimating hemispherical BBE has only been validated under zero wind speed conditions, due to the lack of in situ directional emissivity values measured under different wind speeds. Thus, the deployment of comprehensive field campaigns and the collection of more in situ emissivity measurements are needed.

Acknowledgments: This work was partly supported by the National Natural Science Foundation of China via Grant 41371323 and 41331173, the National High Technology Research and Development Program of China via Grant 2013AA122801, and Beijing Higher Education Young Elite Teacher Project via Grant YETP0233. The Spanish Ministerio de Economía y Competitividad and the European Regional Development Fund (FEDER), through the project CGL2015-64268-R (MINECO/FEDER, UE), were also acknowledged. The MERRA 2 data was obtained from ftp://goldsmr4.sci.gsfc.nasa.gov/data/s4pa/. This study highly profited from the dedicated and very constructive reviewers.

Author Contributions: Xiaolong Cheng and Jie Cheng performed the experiments and wrote the paper; Jie Cheng and Aixiu Nie conceived and designed the experiments; Shunlin Liang and Raquel Niclòs helped in the writing and revision of the manuscript. Qiang Liu analyzed the data.

Conflicts of Interest: The authors declare no conflfigureict of interest.

References

1. McMillin, L.M. Estimation of sea surface temperature from two infrared window measurements with different absorption. *J. Geophys. Res.* **1975**, *20*, 11587–11601. [CrossRef]
2. Niclos, R.; Estrela, M.J.; Valiente, J.A.; Barbera, M.J. Proposal and validation of an emissivity-dependent algorithm to retrieve sea-surface temperature from MSG-SEVIRI data. *IEEE Geosci. Remote Sens. Lett.* **2010**, *7*, 786–790. [CrossRef]
3. Barton, I.J. Satellite-derived sea surface temperatures—A comparison between operational, theoretical and experimental algorithms. *J. Appl. Meteorol.* **1992**, *31*, 432–442. [CrossRef]
4. Kilpatrick, K.A.; Podesta, G.; Walsh, S.; Williams, E.; Halliwell, V.; Szczodrak, M.; Brown, O.B.; Minnett, P.J.; Evans, R. A decade of sea surface temperature from modis. *Remote Sens. Environ.* **2015**, *165*, 27–41. [CrossRef]
5. Niclos, R.; Caselles, V.; Coll, C.; Valor, E. Determination of sea surface temperature at large observation angles using an angular and emissivity dependent split-window equation. *Remote Sens. Environ.* **2007**, *111*, 107–121. [CrossRef]
6. Hanafin, J.A.; Minnett, P.J. Measurements of the infrared emissivity of a wind-roughened sea surface. *Appl. Opt.* **2005**, *44*, 398–411. [CrossRef] [PubMed]
7. Wu, X.; Smith, W.L. Sensitivity of sea surface temperature retrieval to sea surface emissivity. *ACTA Meteorol. Sin.* **1996**, *10*, 376–384.
8. Von Schuckmann, K.; Palmer, M.D.; Trenberth, K.E.; Cazenave, A.; Chambers, D.; Champollion, N.; Hansen, J.; Josey, S.A.; Leob, N.; Mathieu, P.-P.; et al. An imperative to monitor earth's energy imbalance. *Nat. Clim. Chang.* **2016**, *6*, 138–144. [CrossRef]
9. Trenberth, K.E.; Fasullo, J.T.; Balmaseda, M.A. Earth's energy imbalance. *J. Clim.* **2014**, *27*, 3129–3144. [CrossRef]
10. Stephens, G.L.; L'Ecuyer, T. The earth's energy balance. *Atmos. Res.* **2015**, *166*, 195–203. [CrossRef]
11. Cheng, J.; Liang, S.; Yao, Y.; Zhang, X. Estimating the optimal broadband emissivity spectral range for calculating surface longwave net radiation. *IEEE Geosci. Remote Sens. Lett.* **2013**, *10*, 401–405. [CrossRef]
12. Cheng, J.; Liang, S. Effects of thermal-infrared emissivity directionality on surface broadband emissivity and longwave net radiation estimation. *IEEE Geosci. Remote Sens. Lett.* **2014**, *11*, 499–503. [CrossRef]
13. Masuda, K.; Takashima, T.; Takayama, Y. Emissivity of pure and sea waters for the model sea surface in the infrared window regions. *Remote Sens. Environ.* **1988**, *24*, 313–329. [CrossRef]

14. Cox, C.; Munk, W. Statistics of the sea surface derived from sun glitter. *J. Mar. Res.* **1954**, *13*, 198–227.
15. Watts, P.D.; Allen, M.R.; Nightingale, T.J. Wind speed effects on sea surface emission and reflection for the along track scanning radiometer. *J. Atmos. Ocean. Technol.* **1996**, *13*, 126–141. [CrossRef]
16. Wu, X.; Smith, W.L. Emissivity of rough sea surface for 8–13 um: Modeling and verification. *Appl. Opt.* **1997**, *36*, 2609–2619. [CrossRef] [PubMed]
17. Masuda, K. Infrared sea surface emissivity including multiple reflection effect for isotropic Gaussian slope distripution model. *Remote Sens. Environ.* **2006**, *103*, 488–496. [CrossRef]
18. Freund, D.E.; Joseph, R.I.; Donohue, D.J.; Constantikes, K.T. Numerical computations of rough sea surface emissivity using the interaction probability density. *J. Opt. Soc. Am. A* **1997**, *14*, 1836–1849. [CrossRef]
19. Henderson, B.G.; Theiler, J.; Villeneuve, P. The polarized emissivity of a wind-roughened sea surface: A monte carlo model. *Remote Sens. Environ.* **2003**, *88*, 453–467. [CrossRef]
20. Nalli, N.R.; Minnett, P.J.; delst, P.V. Emissivity and reflection model for calculating unpolarized isotropic water surface-leaving radiance in the infrared. I. Theoretical development and calculations. *Appl. Opt.* **2008**, *47*, 3701–3721. [CrossRef] [PubMed]
21. Nalli, N.R.; Minnett, P.J.; Maddy, E.; McMillan, W.W.; Goldberg, M.D. Emissivity and reflection model for calculating unpolarized isotropic water surface-leaving radiance in the infrared. 2: Validation using fourier transform spectrometers. *Appl. Opt.* **2008**, *47*, 4649–4671. [CrossRef] [PubMed]
22. Van Delst, P. JCSDA infrared sea surface emissivity model. In Proceedings of the 13th International TOVS Study Conference, Sainte-Adele, QC, Canada, 29 October–4 November 2003.
23. Hale, G.M.; Querry, M.R. Optical constants of water in the 200-nm to 200-um wavelength region. *Appl. Opt.* **1973**, *12*, 555–563. [CrossRef] [PubMed]
24. Friedman, D. Infrared characteristics of ocean water (1.5–15 microns). *Appl. Opt.* **1969**, *8*, 2073–2078. [CrossRef] [PubMed]
25. Pointer, L.; Dechambenoy, C. Determination des constantes optiques del'eau entre 1 et 40 um. *Ann. Geophys.* **1966**, *22*, 633–641.
26. Wieliczka, D.M.; Weng, S.; Querry, M.R. Wedge shaped cell for highly absorbent liquids: Infrared optical constants of water. *Appl. Opt.* **1989**, *28*, 1714–1719. [CrossRef] [PubMed]
27. Niclos, R.; Caselles, V.; Valor, E.; Coll, C.; Sanchez, J.M. A simple equation for determining sea surface emissivity in the 3-15 um. *Int. J. Remote Sens.* **2009**, *30*, 1603–1619. [CrossRef]
28. Smith, W.L.; Knuteson, R.O.; Revercomb, H.E.; Feltz, W.; Howell, H.B.; Menzel, W.P.; Nalli, N.; Brown, O.B.; Minnett, P.J.; McKeown, W. Observations of the infrared radiative properties of the ocean—Implications for the measurement of sea surface temperature via satellite remote sensing. *Bull. Am. Meteorol. Soc.* **1996**, *77*, 41–51. [CrossRef]
29. Niclos, R.; Valor, E.; Caselles, V.; Coll, C.; Sanchez, J.M. In situ angular measurements of thermal infrared sea surface emissivity—Validation of models. *Remote Sens. Environ.* **2005**, *94*, 83–93. [CrossRef]
30. Niclos, R.; Caselles, V.; Coll, C.; Valor, E.; Rubio, E. Autonomous measurements of sea surface temperature using in situ thermal infrared data. *J. Atmos. Ocean. Tech.* **2004**, *21*, 683–692. [CrossRef]
31. Niclos, R.; Dona, C.; Valor, E.; Bisquert, M. Thermal-infrared spectral and angular characterization of crude oil and seawater emissivities for oil slick identification. *IEEE Trans. Geosci. Remote Sens.* **2014**, *52*, 5387–5395. [CrossRef]
32. Niclos, R.; Caselles, V.; Valor, E.; Coll, C. Foam effect on the sea surface emissivity in the 8–14 um region. *J. Geophys. Res.* **2007**, *112*. [CrossRef]
33. Branch, R.; Chickadel, C.C.; Jessup, A.T. Infrared emissivity of seawater and foam at large incidence angles in the 3–14 um wavelength range. *Remote Sens. Environ.* **2016**, *184*, 15–24. [CrossRef]
34. Ogawa, K.; Schmugge, T.; Jacob, F.; Prench, A. Estimation of broadband land surface emissivity from multi-spectral thermal infrared remote sensing. *Agronomie* **2002**, *22*, 695–696. [CrossRef]
35. Hapke, B. *Theory of Reflectance and Emittance Spectroscopy*; Cambridge Unviersity Press: New York, NY, USA, 1993.
36. Cheng, J.; Liang, S.; Verhoef, W.; Shi, S.; Liu, Q. Estimating the hemispherical broadband longwave emissivity of global vegetated surfaces using a radiative transfer model. *IEEE Trans. Geosci. Remote Sens.* **2016**, *54*, 905–917. [CrossRef]

37. Anguelova, M.D.; Bettenhausen, M.H.; Gaiser, P.W. Passive remote sensing of sea foam using physically-based models. In Proceedings of the IEEE International Geoscience and Remote Sensing Symposium, Denver, CO, USA, 31 July–4 August 2006; pp. 3676–3679.
38. Wu, J. Variations of whitecap coverage with wind stress and water temperature. *J. Phys. Ocean.* **1988**, *18*, 1064–1068. [CrossRef]
39. Duan, Q.Y.; Gupta, V.K.; Sorooshian, S. Shuffled complex evolution approach for effective and efficient global minimization. *J. Optim. Theory Appl.* **1993**, *3*, 501–521. [CrossRef]
40. Wilber, A.C.; Kratz, D.P.; Gupta, S.K. Surface Emissivity Maps for Use in Satellite Retrievals of Longwave Radiation. Available online: https://ntrs.nasa.gov/archive/nasa/casi.ntrs.nasa.gov/19990100634.pdf (accessed on 5 March 2017).
41. Lee, H.-T.; Laszlo, I.; Gruber, A. *ABI Earth Radiation Budget-Surface Upward Longwave Radiation Algorithm Theoretical Basis Document (ATBD)*; NOAA NESDIS Center for Satellite Applications and Research (STAR): College Park, MD, USA, 2009.
42. Hanafin, J.A. On Sea Surface Properties and Characteristics in the Infrared. Ph.D. Thesis, University of Miami, Coral Gables, FL, USA, August 2002.
43. Embury, W.; Merchant, C.J.; Filipiak, M.J. A reprocessing for climate of sea surface temperature from the along-track scanning radiometers: Basis in radiative transfer. *Remote Sens. Environ.* **2012**, *116*, 32–46. [CrossRef]
44. Newman, S.M.; Smith, J.A.; Glew, M.D.; Rogers, S.M.; Taylor, J.P. Temperature and salinity dependence of sea surface emissivity in the thermal infrared. *Q. J. R. Meteorol. Soc.* **2005**, *131*, 2539–2557. [CrossRef]